

Electron-correlated study of excited states and absorption spectra of some low-symmetry graphene quantum dots

Samayita Das and Alok Shukla

*Department of Physics, Indian Institute of Technology Bombay, Powai, Mumbai 400076, India**

(Dated:)

We have computed the linear optical absorption spectra of three graphene quantum dots (GQDs), saturated by hydrogens on the edges, using both first-principles time-dependent density-functional theory (TDDFT) and the Pariser-Parr-Pople (PPP) model coupled with the configuration-interaction (CI) approach. To understand the influence of electron-correlation effects, we have also calculated the singlet-triplet energy gap (spin gap) of the three GQDs. Because of the presence of edge hydrogens, these GQDs are effectively polycyclic aromatic hydrocarbons (PAHs) dibenzo[bc,ef]coronene (also known as benzo(1,14)bisanthene, $C_{30}H_{14}$), and two isomeric compounds, dinaphtho[8,1,2abc;2',1',8'klm]coronene and dinaphtho[8,1,2abc;2',1',8'jkl]coronene with the chemical formula $C_{36}H_{16}$. The two isomers have different point group symmetries, C_{2v} , and C_{2h} , therefore, this study will also help us understand the influence of symmetry on optical properties. A common feature of the absorption spectra of the three GQDs is that the first peak representing the optical gap is of low to moderate intensity, while the intense peaks appear at higher energies. For each GQD, PPP model calculations performed with the screened parameters agree well with the experimental results of the corresponding PAH, and also with the TDDFT calculations.

I. INTRODUCTION

The electronic structure of an isolated monolayer of graphite, called graphene in the modern times, was studied long ago within the tight-binding model by Wallace, who demonstrated the linear dispersion of the system in the Brillouin zone, and its Dirac cone like structure [1]. Indeed, within a few years of its synthesis 2004[2], graphene became one of the most studied quantum material in general, and Dirac material, in particular [3]. Graphene is noteworthy for its remarkable transport properties because of the massless charge carriers and a very high mobility [2]. However, given the vanishing band gap of graphene, its applications in the field of optoelectronics are limited. For example, graphene, in its pristine form, cannot be used in the light-emitting diodes (LEDs), transistors, switching devices, *etc.* Therefore, there has been significant research in the field to introduce a gap in graphene by chemical modifications such as oxidation, hydrogenation, and heteroatom doping [4–6]. Another way to introduce a gap is by achieving quantum confinement by breaking the translation symmetry of graphene and considering its finite-sized fragments referred to as nano-flakes, nano-disks, and graphene quantum dots (GQDs) [7–9]. The problem with the finite-sized fragments is that they will undergo edge reconstruction to saturate the dangling bonds, and the resulting structure could be highly asymmetric and nonplanar. Therefore, in order to keep a fragment planar, the dangling bonds on its edges need to be passivated. If the interior of a fragment contains multiple aromatic rings, and its dangling bonds are saturated by the hydrogen atoms, the resultant structure will continue to be fully planar, and chemically speaking it will be nothing but a polycyclic aromatic hydrocarbon (PAH). Therefore, fully planar edge-hydrogenated GQDs are nothing but PAHs, and this has been realized by authors in the past who argued that suitably chosen PAHs can be used as models of mono- and multilayer graphite fragments [10]. Because of this close correspondence, the planar edge-hydrogenated GQDs and PAHs are simply synonymous. Therefore, in this work we study the electronic structure and optical properties of three PAHs of somewhat lower point-group symmetries as models of corresponding planar GQDs.

Because of their strictly planar geometry and aromatic character, PAHs are π -conjugated organic molecules in which the energetically low-lying σ -bonds hold the atomic skeleton together, while the orbitals close to the Fermi level are of the π type. PAHs are abundant in nature because they are not only found in fossil fuels on earth, but also in the interstellar dust and are believed to be responsible for the near infrared (IR) to visible absorption bands called diffuse interstellar bands [11]. Because of this reason, the electronic structure, vibrational and optical properties of PAHs have been of great interest not only in physics and chemistry, but also in astronomy and astrophysics [10, 11]. Given the itinerant character of the π electrons, their response to externally applied electromagnetic field is strong, leading to interesting linear and nonlinear optical properties of PAHs. As a result of which, PAHs (or GQDs), have tremendous potential applications in optoelectronic devices [12–19]. Due to their interesting photophysical properties,

* samayitadas5@gmail.com, shukla@iitb.ac.in

PAHs can also be used as solute polarity probes [20]. In addition, it is a well-known fact that many PAHs are highly carcinogenic, therefore, it is important to study their electronic structure and related properties so as to understand their interaction with living tissues [10, 21].

In this work we have studied the optical and electronic properties of three polycyclic aromatic hydrocarbons (PAHs), namely, dibenzo[bc,ef]coronene which is also known as 1.14-benzobisanthrene ($C_{30}H_{14}$), dinaphtho[8,1,2abc;2',1',8'klm]coronene ($C_{36}H_{16}$) and dinaphtho[8,1,2abc;2',1',8'jkl]coronene ($C_{36}H_{16}$), schematics of which are shown in Fig. 1. For the purpose we have used both the first-principles density-functional theory (DFT) based approach as well as the effective π -electron methodology based on Pariser-Parr-Pople (PPP) Hamiltonian [22, 23]. Among the three different PAHs, the last two molecules with 11 aromatic rings have the same chemical formula $C_{36}H_{16}$ as they are isomers of each other, but their optical absorption spectra are quite different because of different point-group symmetries. We find very good agreement between our calculated absorption spectra and the experimental ones reported by Clar and Schmidt[24], Fetzner [25], and Bryson *et al.* [26].

The remainder of the paper is organized as follow. In the next section we describe our computational methodology, while in sec. III we present and discuss our results. Finally, we summarize our conclusions in sec. IV

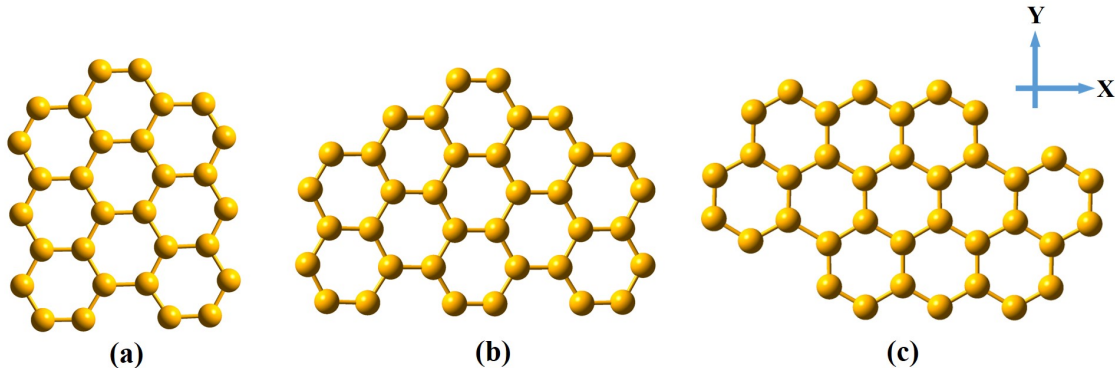


Figure 1. Schematic diagrams of the polycyclic aromatic hydrocarbons (PAHs) considered in this study: (a) dibenzo[bc,ef]coronene ($C_{30}H_{14}$, GQD-30- C_{2v}), (b) dinaphtho[8,1,2abc;2',1',8'klm]coronene ($C_{36}H_{16}$, GQD-36- C_{2v}), (c) dinaphtho[8,1,2abc;2',1',8'jkl]coronene ($C_{36}H_{16}$, GQD-36- C_{2h}). All the molecules are assumed to be lying in the xy plane, as shown. In the parentheses, in addition to the chemical formula of the given PAH, we have assigned a short notation of the form GQD- N - PG , where N denotes the total number of carbon atoms in the PAH, and $PG = C_{2v}$ or C_{2h} , is its point group.

II. COMPUTATIONAL DETAILS

Next we briefly describe the DFT-based first-principles approach along with the PPP-model based configuration interaction (CI) approach, that we employed to study the optical properties of the H-saturated GQDs.

A. First-Principles Approach

The first-principles approach used by us is based on the DFT methodology as implemented in the Gaussian-basis-functions based Gaussian16 package [27]. For a given calculation, besides the basis set, one also has to choose a suitable exchange correlation potential. In our calculations, for all the three molecules, we chose the valence double zeta 6-31++G(d,p) basis set which includes polarization and diffuse functions [28, 29], coupled with the hybrid functional B3LYP [30-32].

The first step of calculations on a given molecule is always the geometry optimization. Convergence criteria of 10^{-8} Hartree was set to self consistently solve Kohn-Sham equations [33]. The geometry of a molecule was considered converged only after the maximum force on an atom, average (RMS) force, maximum displacement, and the average (RMS) displacement were less than 0.00045 Hartree/Bohr, 0.00030 Hartree/Bohr, 0.0018 Bohr, and 0.0012 Bohr, respectively. Even though all the three GQDs considered in this work are well known molecules (PAHs), we still confirmed the stability of their computed structures by performing vibrational frequency analysis, in which no imaginary frequencies were found.

In order to compute the optical absorption spectrum of a GQD, we need to know the excitation energies of its excited states along with their transition dipole couplings to the ground state. For the purpose, we used the time-

dependent density-functional-theory (TDDFT) approach as implemented in Gaussian16 [27], along with the same exchange correlation functional (B3LYP) that were used for the ground state geometry optimization.

B. PPP Model Based Approach

In addition to the first-principles approach described above, we have also used an effective π -electron approach to compute the low-lying excited states and the optical absorption spectra of the molecules considered in this work. Next, we briefly describe the underlying model Hamiltonian, its parameterization, and the electron-correlated configuration interaction approach employed to compute the optical spectra of the considered GQDs.

1. The Hamiltonian and its parameters

In π -conjugated materials, σ and π electrons are well separated in energies, with the π electrons being itinerant and close to the Fermi level, while the σ electrons being highly localized with the energies away from the Fermi level. Based on this concept of $\sigma - \pi$ separation, Pariser, Parr, and Pople argued that the low-lying excited states of the π -conjugated systems can be described by an effective π -electron model Hamiltonian, now known as the PPP Hamiltonian [22, 23], which can be written in the second-quantized form as

$$H = \sum_{i,j,\sigma} t_{ij}(c_{i\sigma}^\dagger c_{j\sigma} + c_{j\sigma}^\dagger c_{i\sigma}) + U \sum_i n_{i\uparrow} n_{i\downarrow} + \sum_{i<j} V_{ij}(n_i - 1)(n_j - 1), \quad (1)$$

where $c_{i\sigma}^\dagger$ ($c_{i\sigma}$) is the creation (annihilation) operator which creates (annihilates) a π -electron with spin σ localized on the i^{th} carbon atom, while the number of π electrons with spin σ is indicated by $n_{i\sigma} = c_{i\sigma}^\dagger c_{i\sigma}$, and $n_i = \sum_\sigma n_{i\sigma}$ denotes the total number of π electrons on the i^{th} carbon atom. Each carbon atom contributes a single π orbital to the basis set, which, for the systems lying in the xy plane, is nothing but the p_z orbital of the atom. In the first term of Eq. 1, t_{ij} represents the one electron hopping matrix element, while U and V_{ij} in the second and third terms denote the onsite, and long-range Coulomb interactions, respectively. Similar to our previous calculations on π -conjugated materials, we only considered nearest-neighbor hopping matrix elements to be non-zero [34–38] whose values were determined using the formula proposed by Ramasesha and coworkers[39]

$$t_{ij} = -2.4 + 3.2(R_{i,j} - 1.397), \quad (2)$$

where $R_{i,j}$ is the distance between the i^{th} and j^{th} carbon atoms in \AA units. Note that, unlike the first-principles approach, in the PPP model hydrogen atoms are not considered because they participate only in the σ bonds.

Ohno relationship is used to parameterize the Coulomb interactions [40]

$$V_{ij} = U/\kappa_{i,j}(1 + 0.6117R_{i,j}^2)^{1/2}, \quad (3)$$

where $\kappa_{i,j}$ denotes dielectric constant of the system, using which we can include the screening effects, and $R_{i,j}$ is the same as in Eq. 2. The positions of various carbon atoms required to compute $R_{i,j}$ were obtained by performing geometry optimization using a first-principles DFT approach discussed in the previous section. In this work, PPP calculations were performed using two sets of Coulomb parameters: (a) the standard parameters [$U = 11.13$ eV, $\kappa_{i,j} = 1.0$], and (b) the screened parameters [$U = 8.0$ eV, $\kappa_{i,j} = 2.0$ ($i \neq j$) and $\kappa_{i,i} = 1.0$] [41].

2. CI Calculations: Computational Steps

A calculation is started by performing a restricted Hartree-Fock (RHF) calculation for the closed-shell singlet ground states of the PAH molecules considered here, by using a computer program implementing the PPP model, developed in our group [42]. The molecular orbitals (MOs) obtained from the RHF calculations are next used to transform the PPP Hamiltonian from the site basis, to the molecular orbital (MO) basis, for performing electron-correlated calculations using the configuration interaction (CI) approach. Next, symmetry- and spin-adapted singles-doubles CI (SDCI) calculations are performed using the computer program MELD [43], to compute the ground and the electric-dipole allowed excited state energies and many-electron wave functions. Subsequently, the transition dipole moments

connecting the ground to the excited states are computed and used to evaluate the optical absorption spectrum of the molecule employing the formula

$$\sigma(\omega) = 4\pi\alpha \sum_n \frac{\omega_{ng} |\langle n | \hat{\mathbf{e}} \cdot \mathbf{r} | g \rangle|^2 \gamma^2}{(\omega_{ng} - \omega)^2 + \gamma^2}, \quad (4)$$

where $|g\rangle$ ($|n\rangle$) denotes the ground (excited) state CI wave function, $\hbar\omega_{ng} = E_n - E_g$ is the energy difference between the two states, $\langle n | \hat{\mathbf{e}} \cdot \mathbf{r} | g \rangle$ is the corresponding transition dipole matrix element for an incident photon of energy $\hbar\omega$ polarized along the $\hat{\mathbf{e}}$ direction, α denotes the fine-structure constant, and γ is the assumed uniform line width for all the excited states. Next we examine the excited states contributing to the prominent peaks in the calculated spectrum, and include the dominant configuration state functions contributing to them in our list of reference configurations for performing the multi-reference singles-doubles CI (MRSDCI) calculations in the next step. Subsequently, the absorption spectrum at the MRSDCI level is calculated and compared to the one computed in the previous CI calculation. This procedure is iterated until the absorption spectrum converges within an acceptable tolerance [34–38].

III. RESULTS AND DISCUSSION

From Fig. 1 it is obvious that the point group symmetries of dibenzo[bc,ef]coronene, dinaphtho[8,1,2abc;2',1',8'klm]coronene, and dinaphtho[8,1,2abc;2',1',8'jkl]coronene respectively are C_{2v} , C_{2v} , and C_{2h} . Therefore, in order to represent the PAHs considered in this work succinctly, we have adopted a notation of the form GQD- N - PG , where N denotes the total number of carbon atoms in the PAH, and PG is its point group which can be C_{2v} or C_{2h} in the present case (see the caption of Fig. 1). Therefore, henceforth, dibenzo[bc,ef]coronene, dinaphtho[8,1,2abc;2',1',8'klm]coronene, and dinaphtho[8,1,2abc;2',1',8'jkl]coronene will be denoted as GQD-30- C_{2v} , GQD-36- C_{2v} , and GQD-36- C_{2h} , respectively.

A. Optimized Structures of the GQDs

Optimized geometries of the three GQDs considered in this work are shown in Fig. 2. All the final structures are strictly planar, with the bond lengths and bond angles showing variations close to the ideal values of 1.4 Å and 120°, respectively. For the first molecule (GQD-30- C_{2v}), the minimum and maximum bond lengths are 1.39 Å (C11-C12) and 1.44 Å (C17-C18), while the minimum and maximum bond angles are 119.80° (C2-C3-C6) and 120.60° (C28-C30-C29), respectively. The parentheses following the bond lengths and angles list the carbon atoms involved in those, according to the atom numbering scheme in Fig. 2(a). For GQD-36- C_{2v} (Fig. 2(b)), the minimum and maximum bond lengths and angles are 1.38 Å (C23-C24), 1.43 Å (C1-C7), and 119.91° (C18-C19-C20, C9-C10-C11), 120.30° (C32-C36-C35, C28-C29-C26), respectively. Finally, for GQD-36- C_{2h} (Fig. 2(c)), the corresponding minimum and maximum values are 1.39 Å (C27-C28), 1.43 Å (C8-C9), and 119.64° (C5-C13-C22), 120.36° (C31-C32-C33). For all the three GQDs, all C-H bond lengths at the edges were very close to 1.09 Å. Furthermore, the geometries of the three GQDs even after the optimization process retain the point group symmetries depicted in the schematic diagram of Fig. 1.

B. Size of the PPP-CI Calculations

All the GQDs considered in this work are charge neutral, as a result they correspond to half-filled systems with each carbon atom contributing a single π electron. Therefore, with the total number of electrons in the GQDs being 30 or 36, all of them have a closed-shell singlet ground state corresponding to the symmetric irreducible representation (irrep) of their point group. As a result, the ground-state symmetry of GQD-30- C_{2v} and GQD-36- C_{2v} is 1A_1 , while that of GQD-36- C_{2h} is 1A_g . Within the PPP approach, one can only consider optically excited states corresponding to the transitions caused by photons polarized in the plane of the molecule. Therefore, according to the dipole selection rules of the point groups C_{2v} and C_{2h} , the possible irreps of the one-photon excited states are either 1A_1 or 1B_2 for GQD-30- C_{2v} , GQD-36- C_{2v} , and 1B_u for GQD-36- C_{2h} .

For the calculations of the optical gaps and absorption spectra of various GQDs, a coefficient cutoff value of 0.05 was used in the MRSDCI calculations. This means that all those configurations in the MRSDCI expansion of the targeted state (ground or the excited state) with the coefficients larger in magnitude than 0.05 are included in the list of the reference configurations in the next iteration of the MRSDCI calculation, and the procedure is repeated

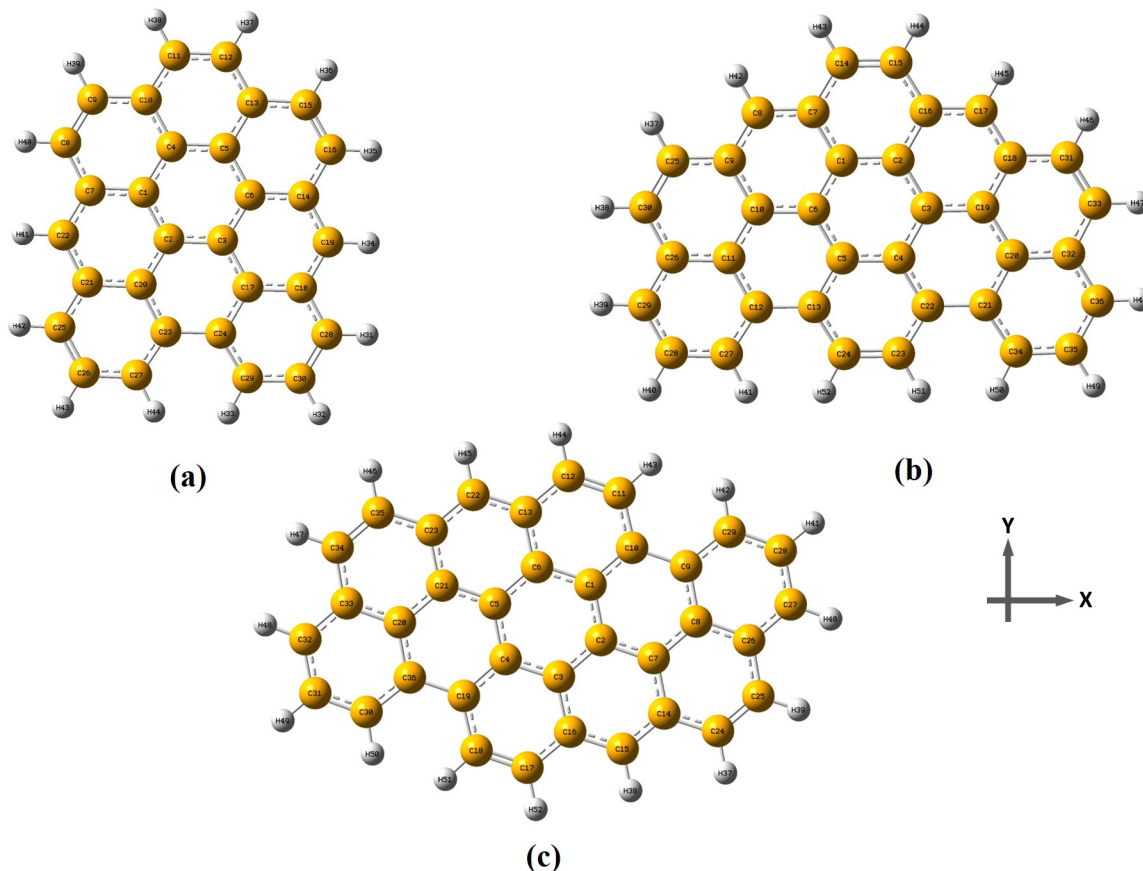


Figure 2. Optimized geometries of the three GQDs: (a) GQD-30- C_{2v} , (b) GQD-36- C_{2v} , and (c) GQD-36- C_{2h} . In the figures, yellow/grey spheres denote C/H atoms.

until the desired quantities converge. For the calculation of the spin gap, i.e., the energy gap between the singlet ground state and lowest-energy triplet state of a GQD, only the two states in question were targeted in the MRSDCI calculations and the calculations were continued until the spin gap converged. As a result we included configurations with a cutoff value 0.03 for the coefficients, leading to significantly larger CI expansions as compared to those needed for the calculation of the absorption spectra. To illustrate the large-scale nature of our CI calculations, the total number of spin-adapted configurations (N_{total}), i.e., the dimension of the CI matrix for the largest calculations of a given symmetry manifold are presented in Table I. From the Table it is obvious that the size of the MRSDCI expansion ranged from close to one million to almost five million, suggesting that our calculations are well-converged.

Table I. Total number of symmetry and spin-adapted configurations (N_{total}) used in the largest PPP-MRSDCI calculations for different symmetries, employing the standard (std) and screened (scr) Coulomb parameters.

GQD	Irrep	$N_{total}(\text{std})$	$N_{total}(\text{scr})$
GQD-30- C_{2v}	1A_1	1283990	1590944
	1B_2	839374	971738
	3B_2	2221359	2641743
GQD-36- C_{2v}	1A_1	1978364	3075530
	1B_2	1427001	1940654
	3B_2	3855805	4078607
GQD-36- C_{2h}	1A_g	3056665	3304115
	1B_u	2314242	1729422
	3B_u	4601107	4820343

C. Optical gaps

We will discuss the computed absorption spectra of the three GQDs in detail in the next section, however, first we discuss their calculated and measured optical gaps, corresponding to the first peaks. In Table II, we present the results of our calculations for the optical gaps of the three GQDs, along with the corresponding experimental results [24–26]. We note that both for the TDDFT as well as PPP-CI calculations, the optical gap corresponds to a many-electron state dominated by HOMO-LUMO singly-excited configuration denoted as $|H \rightarrow L\rangle$. As far as quantitative values are concerned, the gaps computed using the PPP-CI approach coupled with the screened parameters are, on the average, in the best agreement with the solution-based experiments of Clar and Schmidt [24] and Fetzer [25]. However, for the case of GQD-36- C_{2v} , thin-film based measurements of Bryson *et al.* [26] are lower than all the calculated as well as reported values of Fetzer [25]. The possible reason behind this may be the coupling between different molecules (chromophores) in the thin-film phase, leading to a red shift in the first absorption peak as compared to the solution-based results. The gaps computed using the standard parameters in the PPP-CI method overestimate the experimental values for all the cases, while those computed using the first-principles TDDFT method underestimate it for GQD-30- C_{2v} . However, the TDDFT results for GQD-36- C_{2v} and GQD-36- C_{2h} are in very good agreement with the experiment.

Table II. Optical gaps of the three GQDs calculated using the TDDFT method along with PPP-CI approach employing the standard (std) and screened (scr) parameters. The experimental results are also presented for comparison.

Molecules	Optical gap (eV) TDDFT	Optical gap (eV) PPP-CI		Optical gap (eV) Experiment
		scr	std	
GQD-30- C_{2v}	2.22	2.36	2.76	2.46 [24]
GQD-36- C_{2v}	2.79	2.91	3.22	2.67 [26], 2.88 [25]
GQD-36- C_{2h}	2.51	2.53	2.97	2.50 [25]

D. Optical absorption spectra

In this section, we present and analyze the computed linear optical absorption spectra, obtained using both the first-principles TDDFT approach followed by those computed using the PPP model and the MRSDCI approach (PPP-CI approach, in short) for the three PAH molecules considered in this work. For our calculations, the optimized geometries presented in Fig. 2 were utilized. For the chosen orientation of the Cartesian axes, in C_{2v} GQDs, an optical transition from the ground state to a 1B_2 excited states will be through an x -polarized photon, while a transition to a state of 1A_1 symmetry will involve a y -polarized photon. In the C_{2h} GQD, an optical transition from the ground state will be to a state of 1B_u symmetry, through a photon of mixed x, y polarization.

On comparing the PPP-CI spectra of each molecule computed using the standard and the screened parameters, we see the following qualitative similarities: (a) generally speaking, the peaks and features in the spectrum calculated using the screened parameters are at lower excitation energies as compared to the one computed using the standard parameters, (b) the first peaks of the spectra are of weak to moderate intensities corresponding to the optical gap, with the excited states dominated by the $|H \rightarrow L\rangle$ configuration, and (c) for this state, the absorbed photon is x -polarized for the GQDs of the C_{2v} symmetry, and has mixed polarization for the C_{2h} symmetric GQD.

Having already discussed the locations of the first peaks (optical gap) in the absorption spectra in the previous section, here we focus on the higher energy peaks, and, in particular, the maximum intensity (MI) peaks, whose excitation energies are presented in Table III.

Table III. The positions of the most intense (MI) peaks in the optical absorption spectra of the GQDs considered in this work, computed using different approaches, compared to the corresponding experimental values. The peak number and polarization direction of the MI peak are indicated in the parentheses.

GQD	Most intense peak (eV)			
	TDDFT	PPP-CI (scr)	PPP-CI (std)	Experiment (eV)
GQD-30- C_{2v}	3.83 (III _y)	3.41 (II _y)	4.29 (II _y)	3.74 [24]
GQD-36- C_{2v}	3.34 (II _{xy})	3.17 (II _{xy})	3.94 (II _{xy})	3.29 [26], 3.42 [25]
GQD-36- C_{2h}	3.40 (II _{xy})	3.22 (II _{xy})	4.05 (II _{xy})	3.41 [25]

The detailed information regarding the excitations and the wave functions contributing to the peaks of the optical absorption spectra of all the three molecules are presented in tables S1-S9 of the supporting information (SI).

1. GQD-30- C_{2v}

TDDFT Spectrum

In Fig. 3 we present the linear optical absorption spectrum of GQD-30- C_{2v} computed using the TDDFT approach coupled with the B3LYP functional. The spectrum has four features, of which the first peak located at 2.22 eV is due to the absorption of a photon with polarization along the x direction, to a state whose wave function is dominated by the $|H \rightarrow L\rangle$ configuration. As far as the intensity profile of the absorption spectrum is concerned, the first peak is not the most intense, rather it is the y -polarized third peak located at 3.83 eV which is the most intense one. The experimentally measured location of the most intense peak at 3.74 eV [24] is in a very good agreement with this value. The dominant configuration contributing to the excited state giving rise to this peak (III) is $|H \rightarrow L + 3\rangle$, while those contributing to the shoulder II and the weak peak IV are $|H - 3 \rightarrow L\rangle$, and $|H - 1 \rightarrow L + 1\rangle$, respectively. The detailed information about the excited states contributing to the spectrum is presented in Table S1 of SI.

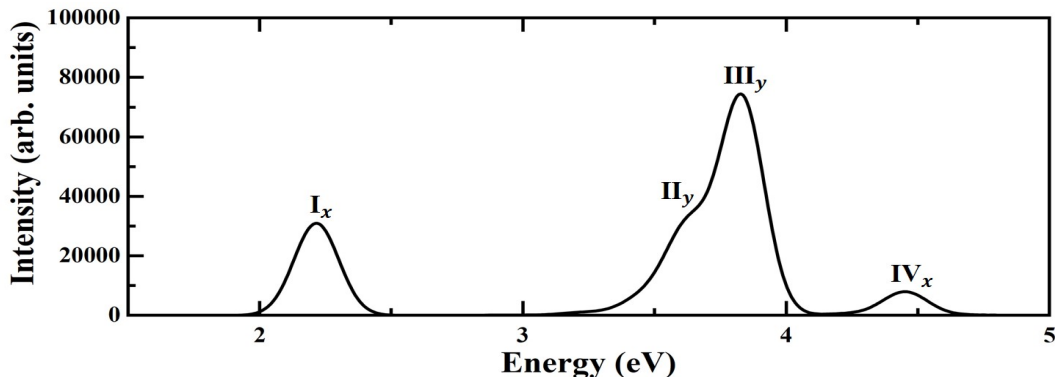


Figure 3. UV-Vis absorption spectrum of GQD-30- C_{2v} , i.e., dibenzo[bc,ef]coronene ($C_{30}H_{14}$), computed using the first-principles TDDFT method. The subscript associated with each peak label indicates the direction of polarization of the absorbed photon.

PPP-CI Spectra

We present PPP-CI level calculated linear optical absorption spectra of GQD-30- C_{2v} employing both the standard and the screened Coulomb parameters presented in Fig. 4. For both the calculations, the second peak (II) corresponding to a y -polarized transition is the MI peak, with the excited states dominated by the singly excited configurations $|H - 1 \rightarrow L\rangle + c.c.$, where $c.c.$ denotes the charge-conjugated configuration $|H \rightarrow L + 1\rangle$. As far as quantitative comparison among the approaches on location of the MI peak is concerned (see Table III), the PPP-CI value 3.41 eV computed using the screened parameters is about 0.4 eV lower than the location of peak III at 3.83 eV in TDDFT spectrum. However, if we consider the MI peak to be a broad band starting at peak II in the TDDFT

spectrum located at 3.63 eV, the difference reduces to about 0.2 eV. The PPP-CI location of the MI peak based on the standard parameter calculations at 4.29 eV, is about 0.5 eV higher than the TDDFT value. Compared to the experimental location of the MI peak at 3.74 eV [24], our screened parameter value is about 0.3 eV lower while the standard parameter value is about 0.6 eV higher.

After the MI peak, the next significant high intensity peak in the screened parameter spectrum occurs at 4.70 eV (peak V) due to two almost degenerate excited states with x and y polarizations. The wave function of the y -polarized state is dominated by single excitations $|H - 6 \rightarrow L\rangle + c.c.$ while the x -polarized state is mainly composed of the single excitation $|H - 2 \rightarrow L + 2\rangle$ with small contribution from the triple excitation $|H \rightarrow L; H \rightarrow L; H - 2 \rightarrow L + 2\rangle$ indicating some influence of electron-correlation effects. The y -polarized peak VIII located at 5.48 eV also carries significant oscillator strength and is largely due to the single excitations $|H - 1 \rightarrow L + 5\rangle + c.c.$ Detailed information about all the peaks in the screened parameter spectrum is given in Table S5 of SI.

In the standard parameter spectrum, beyond the MI peak, there is a absorption band of width ≈ 1 eV starting near 5.5 eV and ending close to 6.5 eV with several closely-spaced high intensity peaks. Of these, peaks VII and IX carry maximum intensities, and exhibit both x and y polarization due to nearly degenerate states of 1A_1 and 1B_2 symmetries. Peak VII is dominated by states with single excitations $|H - 6 \rightarrow L\rangle + c.c.$, $|H - 2 \rightarrow L + 2\rangle$, and $|H - 3 \rightarrow L + 3\rangle$, while single excitations $|H - 9 \rightarrow L\rangle + c.c.$, $|H - 4 \rightarrow L + 4\rangle$, $|H - 1 \rightarrow L + 5\rangle + c.c.$, and the triple excitation $|H \rightarrow L; H - 4 \rightarrow L + 1; H - 1 \rightarrow L + 4\rangle$ give rise to peak IX.

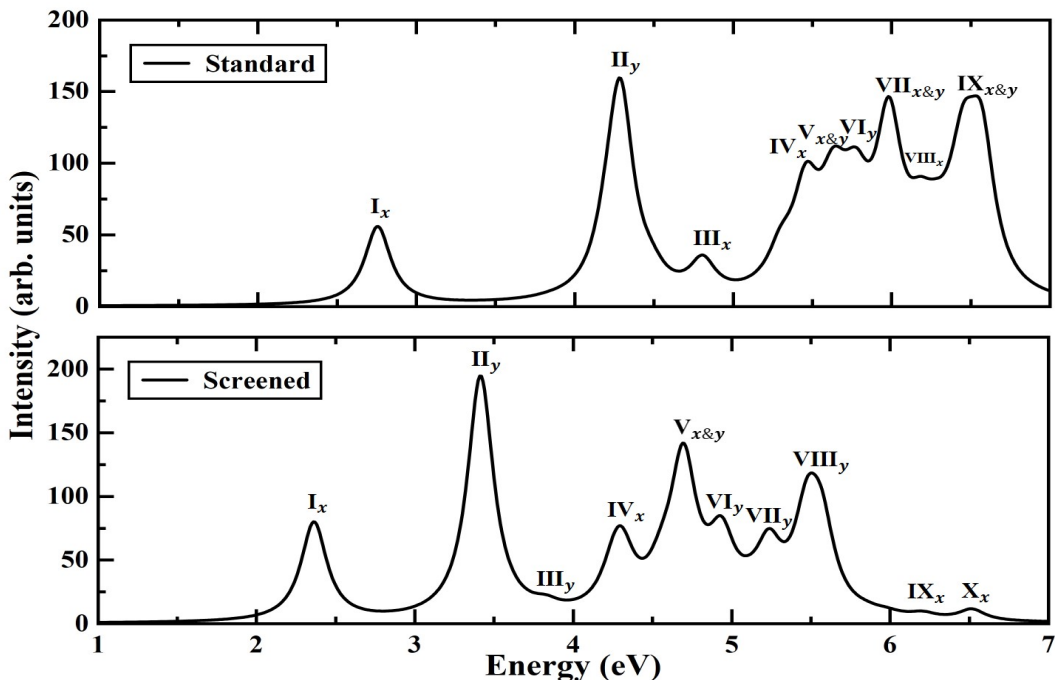


Figure 4. Linear optical absorption spectra of GQD-30- C_{2v} , i.e., dibenzo[bc,ef]coronene ($C_{30}H_{14}$) computed using the PPP-CI methodology. The calculations were performed using the standard parameters (upper panel) and the screened parameters (lower panel) using a uniform line width of 0.1 eV. Polarization directions of the transitions are specified by the subscripts of the peak labels.

One may wonder as to why the absorption spectra computed using the PPP-CI approach (Fig. 4) have so many more peaks as compared to the TDDFT spectrum of Fig. 3. The reason is that the PPP-CI calculations involve many more excited states as compared to the TDDFT calculation, consequently the energy range covered in PPP-CI spectra is about 7 eV as compared to about 4.5 eV in the TDDFT spectrum. If we compare the two sets of spectra up to the excitation energy range 4.5 eV, we note that both the TDDFT and PPP-CI (screened) spectra have four features each, while PPP-CI (standard) has just two features. Furthermore, the polarization directions of those four peaks in TDDFT and PPP-CI (screened) spectra match perfectly with each other. There is also a decent quantitative agreement also in the peak locations predicted by the two spectra. For example, peak IV of TDDFT is located at 4.45 eV while the same peak of PPP-CI (screened) spectrum is at 4.30 eV. Therefore, we conclude that the first-principles TDDFT spectrum is in good qualitative and quantitative agreement with that computed by the PPP-CI (screened) approach.

2. GQD-36- C_{2v}

TDDFT Spectrum

We present the linear optical absorption spectrum of GQD-36- C_{2v} , computed using the TDDFT approach, in Fig. 5. We have identified six features in the spectrum with the maximum excitation energy ≈ 4.6 eV. The first peak corresponding to the optical gap is due to an excited state whose many-body wave function is dominated by the $|H \rightarrow L\rangle$ excitation, and similar to the case of GQD-30- C_{2v} , it is also reached by the absorption of an x -polarized photon. The most intense peak of the computed spectrum is peak II located at 3.34 eV with mixed x and y polarizations due to two closely-spaced excited states of symmetries 1B_2 and 1A_1 whose wave functions are dominated by single excitations $|H - 1 \rightarrow L + 1\rangle$, and $|H \rightarrow L + 1\rangle$, respectively. To the oscillator strength of this peak, the x -polarized 1B_2 contributes significantly more as compared to the y -polarized 1A_1 state. As far as the location of the MI peak is concerned, the TDDFT value (3.34 eV) is again in good agreement with the experimental values 3.29 eV and 3.42 eV reported by Bryson *et al.* [26], and Fetzner [25], respectively. In the region beyond the MI peak, there are four weaker peaks of which the x -polarized peak IV near 4.07 eV carries significant intensity, and is dominated by the excitation $|H - 2 \rightarrow L + 1\rangle$. The last peak (peak VI) of the computed spectrum is slightly above 4.5 eV and is quite feeble. The detailed information about the excited states contributing to the spectrum of this QD can be found in Table S2 of SI.

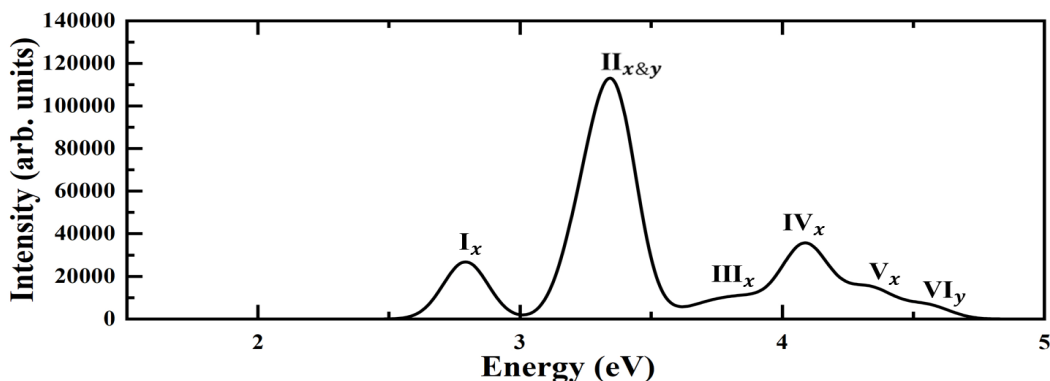


Figure 5. UV-Vis absorption spectrum of GQD-36- C_{2v} , i.e., dinaphtho[8,1,2abc;2',1',8'klm]coronene ($C_{36}H_{16}$), computed using the first-principles TDDFT method. The subscript associated with each peak label indicates the direction of polarization of the absorbed photon.

PPP-CI Spectra

We present the linear optical absorption spectra of GQD-36- C_{2v} computed using the PPP-CI approach, employing both sets of Coulomb parameters, in Fig. 6. The first peak in the spectrum computed using the standard parameters is of very low intensity while the corresponding peak in the screened parameter spectrum is of moderate intensity.

In both the spectra, the second peak is the MI peak, which derives large oscillator strengths from two nearly degenerate excited states of 1B_2 and 1A_1 symmetries, whose wave functions are dominated by single excitations $|H - 1 \rightarrow L + 1\rangle$, and $|H \rightarrow L + 1\rangle + c.c.$, respectively. The PPP-CI (screened) location of the MI peak at 3.17 eV is slightly smaller than the corresponding TDDFT value of 3.34 eV, while the standard parameter location of the MI peak at 3.94 eV is significantly larger than it (see Table III)

In the screened parameter spectrum, beyond the MI peak there are several features of which peak III near 4.0 eV is close to an experimental peak around 3.9 eV [25]. Similarly, peaks IV (4.22 eV) and V (4.44 eV) of this spectrum are close to experimental peaks located at 4.26 and 4.30 eV, respectively [25]. In the computed spectrum there are two more peaks VI (5.07 eV) and VII (5.33 eV) of significant intensities, that are y - and x -polarized, with their many-body wave functions dominated by the single excitations $|H - 3 \rightarrow L + 2\rangle + c.c.$ and $|H - 4 \rightarrow L + 3\rangle + c.c.$, respectively. Of these, peak VI (5.07 eV) is close to an experimentally measured strong peak near 5 eV [25]. Additionally, there are several other weaker features in the computed spectrum at energies higher than 5.0 eV.

In the PPP-CI (standard) spectrum, the MI peak is followed by a number of weak-intensity peaks. The next intense peak (X) is of mixed polarization and occurs due to three closely-spaced states at 6.32 eV (1B_2), 6.41 eV (1B_2), and 6.49 eV (1A_1), dominated by excitations $|H - 3 \rightarrow L + 3\rangle$, $|H - 2 \rightarrow L + 5\rangle + c.c.$, and $|H - 2 \rightarrow L + 3\rangle + c.c.$

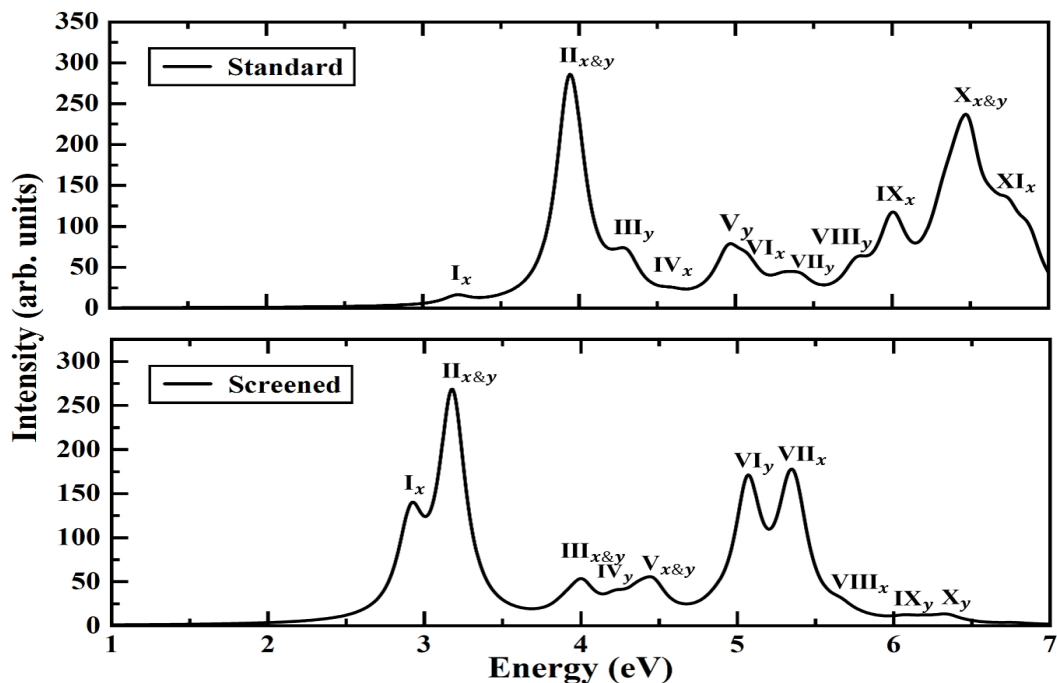


Figure 6. Linear optical absorption spectra of GQD-36- C_{2v} , i.e., dinaphtho[8,1,2abc;2',1',8'klm]coronene ($C_{36}H_{16}$) computed using the PPP-CI methodology. The calculations were performed using the standard parameters (upper panel) and the screened parameters (lower panel) using a uniform line width of 0.1 eV. Polarization directions of the transitions are specified by the subscripts of the peak labels.

We note that the TDDFT spectrum of this molecule has six features in all extending up to slightly beyond 4.5 eV (see Fig. 5). In that energy region PPP-CI (screened) spectrum has five features while the standard parameter spectrum has four. The polarization characteristics of the first two peaks are in agreement in all the three spectra, and the intensity profiles also match in this energy region because beyond the MI peak and below 4.5 eV, the peaks are quite feeble in all the three spectra.

3. GQD-36- C_{2h}

TDDFT Spectrum

Fig. 7 presents the linear optical absorption spectrum of GQD-36- C_{2h} computed using the TDDFT approach and the B3LYP functional. The spectrum displays four well-defined peaks, all of which have mixed polarization characteristics in agreement with the electric-dipole selection rules of the C_{2h} point group. The first peak located at 2.51 eV is due to a state whose wave function is dominated by the $|H \rightarrow L\rangle$ configuration, while the second peak at 3.40 eV is the MI peak whose wave function is mainly composed of the single excitation $|H - 1 \rightarrow L\rangle$. The TDDFT location of the MI peak (3.40 eV) is in excellent agreement with the experimental value 3.41 eV reported by Fetzer [25].

The third and the fourth peaks of the spectrum located at 3.84 and 4.24 eV are as intense as the first peak, and are due to excited states dominated by single excitations $|H - 1 \rightarrow L + 1\rangle$, and $|H - 2 \rightarrow L + 2\rangle$, respectively. More details about the excited states contributing to the spectrum can be found in Table S3 of SI.

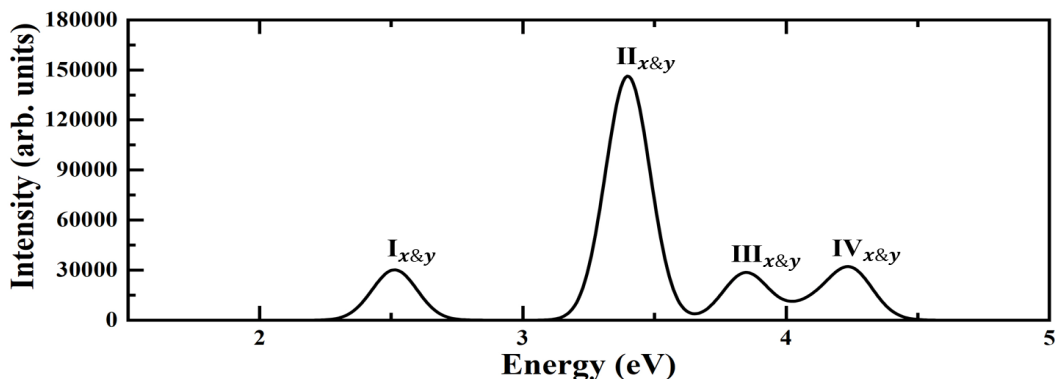


Figure 7. UV-Vis absorption spectrum of GQD-36- C_{2h} , i.e., dinaphtho[8,1,2abc;2',1',8'jkl]coronene ($C_{36}H_{16}$), computed using the first-principles TDDFT method. The subscript associated with each peak label indicates the direction of polarization of the absorbed photon.

PPP-CI Spectra

The optical absorption spectra of GQD-36- C_{2h} computed using the PPP-CI approach, employing both the standard and screened Coulomb parameters are presented in Fig. 8. The detailed information about the excited states contributing to various peaks can be found in Tables S8 (standard) and S9 (screened) of the SI. The first peak in the spectrum computed using the standard parameters has lower relative intensity as compared the corresponding peak in the screened parameter spectrum.

The MI peak is the second peak (II) in both the spectra, and the state giving rise to it is dominated by $|H \rightarrow L + 1\rangle + c.c.$ singly-excited configurations. As far the location of the MI peak is concerned, the PPP-CI (screened) value of 3.22 eV is slightly smaller than the TDDFT value 3.40 eV, while the PPP-CI (standard) location at 4.05 eV is significantly larger than it (see Table III)

In the standard parameter spectrum, beyond the MI peak there are several moderate-intensity peaks all the way up to 6.5 eV. Out of these, two peaks (III and IV) are below 5 eV, while the remaining five features are above that energy. The wave functions of the states leading to peak III (4.37 eV) and peak IV (4.66 eV) exhibit significant configuration mixing with strong contributions from single excitations $|H - 2 \rightarrow L + 2\rangle$ and $|H - 1 \rightarrow L + 1\rangle$, and $|H - 1 \rightarrow L + 1\rangle$ and $|H - 5 \rightarrow L\rangle + c.c.$, respectively. With the increasing energy of the peaks, the transitions occur to orbitals farther away from the Fermi level. For example, the peaks V (5.34 eV) and IX (6.47 eV) are dominated by excitations $|H \rightarrow L + 8\rangle + c.c.$, and $|H - 4 \rightarrow L + 4\rangle$, respectively.

In the screened parameter spectrum, beyond the MI peak, there are three more moderate intensity peaks (III, IV, and VI) in the region up to 5.0 eV, while the last peak (VII) at 5.75 eV is a very faint one. The excited states contributing to peaks III (3.93 eV), IV (4.33 eV), and VI (5.03 eV) are dominated by the excitations $|H - 1 \rightarrow L + 1\rangle$, $|H - 2 \rightarrow L + 2\rangle$, and $|H - 5 \rightarrow L + 1\rangle + c.c.$, respectively. We also note that in the experimental spectrum [25], peaks at 3.85 eV, 4.30 eV, and 4.70 are very close to the locations of our calculated peaks III (3.93 eV), IV (4.33 eV), and shoulder (V) at 4.79 eV, respectively. More information about the excited states contributing to the PPP-CI spectra can be found in Tables S8 and S9 of the SI for the standard and screened parameter calculations, respectively.

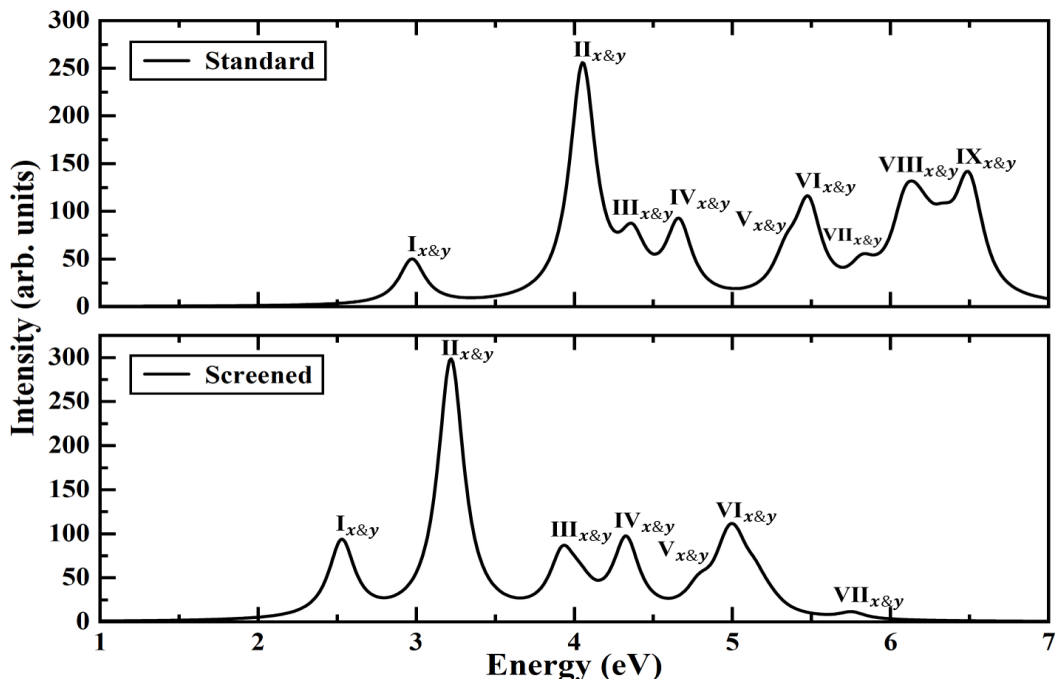


Figure 8. Linear optical absorption spectra of GQD-36- C_{2h} , i.e., dinaphtho[8,1,2abc;2',1',8'jkl]coronene ($C_{36}H_{16}$) computed using the PPP-CI methodology. The calculations were performed using the standard parameters (upper panel) and the screened parameters (lower panel) using a uniform line width of 0.1 eV. Polarization directions of the transitions are specified by the subscripts of the peak labels.

The TDDFT spectrum of this molecule has four peaks in all, the last of which is located at 4.24 eV (see Fig. 7). In that energy range, broadly speaking PPP-CI (screened) spectrum also has four peaks (peak IV is at 4.33 eV), while the standard parameter spectrum has three peaks. Furthermore, peak III of TDDFT spectrum located at 3.84 eV compares very well with the peak III of the screened parameter spectrum at 3.93 eV. Thus, we conclude that the spectra computed by TDDFT and the PPP-CI (screened) approaches are in excellent qualitative and quantitative agreement with each other for GQD-36- C_{2h} .

It is also important to compare the optical properties of GQD-36- C_{2v} and GQD-36- C_{2h} because they are isomeric, as a result of which any differences between them will strictly be due to their structural differences. We note that at all levels of theory and also experiments (see Table II), the optical gap of GQD-36- C_{2v} is larger than that of GQD-36- C_{2h} . However, when it comes to the MI peak, at all levels of theory and experiment their locations for the two molecules are very close to each other (see Table III).

E. Singlet-triplet gap

The singlet-triplet gap, also called the spin gap, defined as the energy difference between the lowest singlet (S_0) and triplet states (T_1) of a given molecule, contains important information about a possible magnetic character as well as electron-correlation effects in the system. In our case, it is defined as $\Delta E_{ST} = E(1^3B_x) - E(1^1A_y)$, here ($x = 2, y = 1$) for the first two molecules with the C_{2v} point group symmetry, and ($x = u, y = g$) for the third molecule with C_{2h} point group symmetry. We saw in the previous section that the many particle wave function of the first singlet state (S_1) optically connected to S_0 is dominated by the single excitation $|H \rightarrow L\rangle$. Similarly, the many-particle wave function of T_1 is also dominated by the same orbital excitation $|H \rightarrow L\rangle$, as a result of which: (a) the many-particle wave function of the T_1 state will have the same point-group symmetry of $B_2(C_{2v})$ or $B_u(C_{2h})$ as that of the corresponding S_1 state, and (b) in the non-interacting tight-binding theory T_1 and S_1 will be degenerate. However, once the electron-electron interactions are taken into account as in the PPP model, the S_1 - T_1 degeneracy gets lifted leading to a spin gap significantly smaller than the optical gap. Thus, it is obvious that the different spin and optical gaps of a system are a consequence of electron-correlation effects. In Table IV, our PPP-CI results for the spin gaps Δ_{ST} for the three molecules are presented from which we conclude: (a) screened parameter based spin gaps are smaller than the standard parameter ones, and (b) spin gap of each molecule is significantly smaller than its optical gap (see Table II) for PPP-CI calculations performed with both Coulomb parameters. On comparing the

Table IV. Singlet-triplet gap, or the spin gap (Δ_{ST}) of various GQDs computed using the PPP-MRSDCI approach using the standard and screened parameters.

GQD	$\Delta_{ST}(\text{eV})$	
	Standard	Screened
GQD-30- C_{2v}	1.52	1.30
GQD-36- C_{2v}	2.20	1.85
GQD-36- C_{2h}	1.84	1.53

spin gaps of the two isomers, similar to their optical gaps, we find the spin gap of GQD-36- C_{2v} to be larger than that of GQD-36- C_{2h} . Given the fact that our PPP-CI (screened) results on the optical gaps and several higher energy features in the absorption spectra of the three GQDs are found to be in very good agreement with the experiments, we expect the same will hold true for spin gaps as well.

IV. CONCLUSIONS

In this paper we presented a systematic, large-scale computational study of the electronic structure and optical properties of three hydrogen-passivated GQDs of low point-group symmetries, i.e., C_{2v} and C_{2h} . These GQDs are also known as coronene derivatives, namely, dibenzo[bc,ef]coronene ($C_{30}H_{14}$), and two isomers, dinaphtho[8,1,2abc;2',1',8'klm]coronene ($C_{36}H_{16}$) and dinaphtho[8,1,2abc; 2',1',8'jkl]coronene ($C_{36}H_{16}$). For the purpose, we employed both the first-principles TDDFT approach, as well as semiempirical PPP model Hamiltonian coupled with the MRSDCI approach. Our optical gaps computed by the PPP-CI approach coupled with the screened parameters were found to be in excellent agreement with the experimental results. However, TDDFT calculations were found to be very accurate in predicting the locations of both the optical gaps as well as most-intense peaks in the spectra of all the three GQDs, when compared to the experiments. Our TDDFT calculations predict the absorption spectrum up to 4.5 eV, while the PPP-CI calculations extend up to 6 eV and beyond. In the PPP-CI spectra computed with the screened parameters, we found several peaks and features that are close to the experimentally measured values for both the isomers of GQD-36. Additionally, within the PPP-CI methodology we also computed the spin gaps of all the three GQDs whose values can be tested in the future experiments.

It will also be useful to study the nonlinear optical response of these systems such as the two-photon absorption and third-harmonic generation. We plan to undertake those calculations in the future along with the influence of doping these systems with heteroatoms.

-
- [1] P. R. Wallace, Phys. Rev. **71**, 622 (1947).
[2] K. S. Novoselov, A. K. Geim, S. V. Morozov, D. Jiang, Y. Zhang, S. V. Dubonos, I. V. Grigorieva, and A. A. Firsov, Science **306**, 666 (2004), <https://www.science.org/doi/pdf/10.1126/science.1102896>.
[3] A. H. Castro Neto, F. Guinea, N. M. R. Peres, K. S. Novoselov, and A. K. Geim, Rev. Mod. Phys. **81**, 109 (2009).
[4] M. Wu, C. Cao, and J. Jiang, Nanotechnology **21**, 505202 (2010).
[5] J. Son, S. Lee, S. J. Kim, B. C. Park, H.-K. Lee, S. Kim, J. H. Kim, B. H. Hong, and J. Hong, Nature communications **7**, 13261 (2016).
[6] P. A. Denis, Chemical Physics Letters **492**, 251 (2010).
[7] L.-s. Li and X. Yan, The Journal of Physical Chemistry Letters **1**, 2572 (2010).
[8] X. Huang, Z. Yin, S. Wu, X. Qi, Q. He, Q. Zhang, Q. Yan, F. Boey, and H. Zhang, small **7**, 1876 (2011).
[9] M. Bacon, S. J. Bradley, and T. Nann, Particle & Particle Systems Characterization **31**, 415 (2014).
[10] S. Canuto, M. C. Zerner, and G. H. F. Diercksen, Astrophys. J. **377**, 150 (1991).
[11] T. R. Geballe, Journal of Physics: Conference Series **728**, 062005 (2016).
[12] B. Lussem, C.-M. Keum, D. Kasemann, B. Naab, Z. Bao, and K. Leo, Chemical reviews **116**, 13714 (2016).
[13] H. Ma, H.-L. Yip, F. Huang, and A. K.-Y. Jen, Advanced Functional Materials **20**, 1371 (2010).
[14] A. Facchetti, Chemistry of Materials **23**, 733 (2011).
[15] F. Guo, A. Karl, Q.-F. Xue, K. C. Tam, K. Forberich, and C. J. Brabec, Light: science & applications **6**, e17094 (2017).
[16] Y. Liu, C. Li, Z. Ren, S. Yan, and M. R. Bryce, Nature Reviews Materials **3**, 1 (2018).
[17] J. C. Fetzler, Polycyclic Aromatic Compounds **27**, 143 (2007).
[18] R. H. Friend, R. Gymer, A. Holmes, J. Burroughes, R. Marks, C. Taliani, D. Bradley, D. D. Santos, J.-L. Bredas, M. Lögdlund, *et al.*, Nature **397**, 121 (1999).
[19] J. H. Burroughes, D. D. Bradley, A. Brown, R. Marks, K. Mackay, R. H. Friend, P. L. Burns, and A. B. Holmes, nature **347**, 539 (1990).

- [20] W. E. Acree, S. A. Tucker, A. I. Zvaigzne, K. W. Street, J. C. Fetzer, and H.-F. Grutzmacher, *Applied spectroscopy* **44**, 477 (1990).
- [21] R. G. Harvey, *Polycyclic aromatic hydrocarbons: chemistry and carcinogenicity* (CUP Archive, 1991).
- [22] J. A. Pople, *Transactions of the Faraday Society* **49**, 1375 (1953).
- [23] R. Pariser and R. G. Parr, *The Journal of Chemical Physics* **21**, 767 (1953).
- [24] E. Clar and W. Schmidt, *Tetrahedron* **33**, 2093 (1977).
- [25] J. C. Fetzer, *Large ($C=24$) polycyclic aromatic hydrocarbons: chemistry and analysis*, Vol. 218 (John Wiley & Sons, 2000).
- [26] K. Bryson, Z. Peeters, F. Salama, B. Foing, P. Ehrenfreund, A. Ricco, E. Jessberger, A. Bischoff, M. Breitfellner, W. Schmidt, and F. Robert, *Advances in Space Research* **48**, 1980 (2011).
- [27] M. J. Frisch, G. W. Trucks, H. B. Schlegel, G. E. Scuseria, M. A. Robb, J. R. Cheeseman, G. Scalmani, V. Barone, G. A. Petersson, and H. N. et. al., *Gaussian 16 revision c.01* (2016), gaussian Inc. Wallingford CT.
- [28] W. J. Hehre, R. Ditchfield, and J. A. Pople, *The Journal of Chemical Physics* **56**, 2257 (1972).
- [29] P. C. Hariharan and J. A. Pople, *Theoretica chimica acta* **28**, 213 (1973).
- [30] C. Lee, W. Yang, and R. G. Parr, *Physical review B* **37**, 785 (1988).
- [31] A. D. Becke, *The Journal of chemical physics* **96**, 2155 (1992).
- [32] A. Becke, *Density-functional thermochemistry. iii. the role of exact exchange*. *j. chem. phys.*, 98: 5648-5652 (1993).
- [33] W. Kohn and L. J. Sham, *Physical review* **140**, A1133 (1965).
- [34] A. Shukla, *Physical Review B* **65**, 125204 (2002).
- [35] A. Shukla, *Physical Review B* **69**, 165218 (2004).
- [36] H. Chakraborty and A. Shukla, *The Journal of Physical Chemistry A* **117**, 14220 (2013).
- [37] H. Chakraborty and A. Shukla, *The Journal of Chemical Physics* **141** (2014).
- [38] P. Bhattacharyya, D. K. Rai, and A. Shukla, *The Journal of Physical Chemistry C* **124**, 14297 (2020).
- [39] M. Das and S. Ramasesha, *Journal of Chemical Sciences* **118**, 67 (2006).
- [40] K. Ohno, *Theoretica chimica acta* **2**, 219 (1964).
- [41] M. Chandross and S. Mazumdar, *Physical Review B* **55**, 1497 (1997).
- [42] P. Sony and A. Shukla, *Computer Physics Communications* **181**, 821 (2010).
- [43] L. McMurchie, S. Elbert, S. Langhoff, and E. Davidson, *It has been modified by us to handle bigger systems* (1990).

Supporting Information:

Electron-correlated study of excited states and absorption spectra of some low-symmetry graphene quantum dots

Samayita Das^{1,*} and Alok Shukla^{1,†}

¹*Department of Physics, Indian Institute of Technology Bombay, Powai, Mumbai 400076, India*

In this supporting information, following tables show the information about the excited states contributing to important peaks in the calculated absorption spectra of the lower-symmetry polycyclic aromatic hydrocarbon molecules considered in this work. The excited state symmetries of the corresponding peaks are also presented below. Here, f ($= \frac{2 \times m_e}{3 \times \hbar^2} (E) \sum_{j=x,y,z} |\langle e | O_j | r \rangle|^2$) indicates the oscillator strength for a particular transition where E , $|e\rangle$, $|r\rangle$ and O_j representing the peak energy, excited states of the corresponding peak, reference state and electric dipole operator for different Cartesian components respectively. In the last column, the numbers inside the bracket represent the contributing coefficients of the wave functions for each corresponding configuration.

Data from TDDFT calculations

Detailed information related to the UV-vis optical absorption spectra of the three GQDs calculated using the TDDFT approach. This includes peak positions E , symmetries of the excited states, oscillator strengths f , polarization direction of the absorbed photon, and the many-body wave functions of the excited states.

Table S1. Information regarding the excited states contributing to the peaks in the linear optical absorption spectrum of GQD-30- C_{2v} (dibenzo[bc,ef]coronene, $C_{30}H_{14}$) computed using the first-principles TDDFT method (Fig. 3, main article). In the 'Peak' column, subscripts x (y) indicate polarization direction of the absorbed photon is along x (y) direction, while xy denotes peaks with contribution from both x and y polarized photon(s).

Peak	Symmetry	E (eV)	f	Wave function
I _{x}	¹ B ₂	2.22	0.23	$ H \rightarrow L\rangle(0.70260)$
II _{y}	¹ A ₁	3.63	0.21	$ H - 3 \rightarrow L\rangle(0.5263)$
III _{y}	¹ A ₁	3.83	0.54	$ H \rightarrow L + 3\rangle(0.39140)$
IV _{x}	¹ B ₂	4.45	0.06	$ H - 1 \rightarrow L + 1\rangle(0.61216)$

Table S2. Information regarding the excited states contributing to the peaks in the linear optical absorption spectrum of GQD-36- C_{2v} (dinaphtho[8,1,2abc;2',1',8'klm]coronene, $C_{36}H_{16}$) computed using the first-principles TDDFT method (Fig. 5, main article). In the 'Peak' column, subscripts x (y) indicate polarization direction of the absorbed photon is along x (y) direction, while xy denotes peaks with contribution from both x and y polarized photon(s).

Peak	Symmetry	E (eV)	f	Wave function
I _{x}	¹ B ₂	2.79	0.20	$ H \rightarrow L\rangle(0.65252)$
II _{xy}	¹ A ₁	3.24	0.30	$ H \rightarrow L + 1\rangle(0.50620)$
	¹ B ₂	3.36	0.71	$ H - 1 \rightarrow L + 1\rangle(0.63007)$
III _{x}	¹ B ₂	3.86	0.05	$ H - 3 \rightarrow L\rangle(0.45941)$
IV _{x}	¹ B ₂	4.07	0.18	$ H - 2 \rightarrow L + 1\rangle(0.43385)$
V _{x}	¹ B ₂	4.33	0.10	$ H - 4 \rightarrow L\rangle(0.47387)$
VI _{y}	¹ A ₁	4.56	0.04	$ H - 6 \rightarrow L\rangle(0.43602)$

* samayitadas5@gmail.com

† shukla@phy.iitb.ac.in

Table S3. Information regarding the excited states contributing to the peaks in the linear optical absorption spectrum of GQD-36- C_{2h} (dinaphtho[8,1,2abc;2',1',8'jkl] coronene, $C_{36}H_{16}$) computed using the first-principles TDDFT method (Fig. 7, main article). In the 'Peak' column, xy indicates the mixed polarization of the absorbed photon.

Peak	Symmetry	E (eV)	f	Wave function
I $_{xy}$	1B_u	2.51	0.22	$ H \rightarrow L\rangle(0.68754)$
II $_{xy}$	1B_u	3.40	1.09	$ H - 1 \rightarrow L\rangle(0.49838)$
III $_{xy}$	1B_u	3.84	0.21	$ H - 1 \rightarrow L + 1\rangle(0.62540)$
IV $_{xy}$	1B_u	4.24	0.23	$ H - 2 \rightarrow L + 2\rangle(0.50781)$

Data from PPP model based calculations

Detailed information related to the UV-vis optical absorption spectra of the three GQDs calculated using the PPP-CI approach. This includes peak positions E , symmetries of the excited states, oscillator strengths f , polarization direction of the absorbed photon, and the many-body wave functions of the excited states.

Table S4. Information regarding the excited states contributing to the peaks in the linear optical absorption spectrum of GQD-30- C_{2v} (dibenzo[bc,ef]coronene, $C_{30}H_{14}$) computed using the PPP-CI method and the standard parameters (Fig. 4, main article). The rest of the information is same as in the caption of Table S1.

Peak	Symmetry	E (eV)	f	Wave function
I $_x$	1B_2	2.76	0.39	$ H \rightarrow L\rangle(0.8528)$ $ H - 1 \rightarrow L + 1\rangle(0.1641)$
II $_y$	1A_1	4.29	1.10	$ H - 1 \rightarrow L\rangle + c.c.(0.5495)$
III $_x$	1B_2	4.81	0.20	$ H - 1 \rightarrow L + 1\rangle(0.5319)$ $ H - 2 \rightarrow L + 2\rangle(0.2664)$
IV $_x$	1B_2	5.46	0.46	$ H - 3 \rightarrow L + 3\rangle(0.4181)$ $ H - 2 \rightarrow L + 2\rangle(0.4062)$
V $_{xy}$	1A_1	5.61	0.47	$ H - 1 \rightarrow L + 2\rangle + c.c.(0.3499)$
	1B_2	5.65	0.48	$ H - 2 \rightarrow L + 2\rangle(0.3281)$ $ H \rightarrow L; H \rightarrow L + 1\rangle + c.c.(0.2480)$
VI $_y$	1A_1	5.78	0.41	$ H - 4 \rightarrow L + 1\rangle + c.c.(0.4716)$
VII $_{xy}$	1A_1	5.98	0.53	$ H - 6 \rightarrow L\rangle + c.c.(0.2649)$
	1B_2	5.99	0.68	$ H - 3 \rightarrow L + 3\rangle(0.4541)$ $ H - 2 \rightarrow L + 2\rangle(0.3634)$
VIII $_x$	1B_2	6.18	0.37	$ H - 2 \rightarrow L + 4\rangle + c.c.(0.4100)$
IX $_{xy}$	1A_1	6.45	0.44	$ H - 9 \rightarrow L\rangle + c.c.(0.3448)$
	1B_2	6.46	0.19	$ H - 4 \rightarrow L + 4\rangle(0.6639)$ $ H \rightarrow L; H - 4 \rightarrow L + 1\rangle + c.c.(0.2161)$
	1A_1	6.57	0.79	$ H - 1 \rightarrow L + 5\rangle + c.c.(0.3942)$

Table S5. Information regarding the excited states contributing to the peaks in the linear optical absorption spectrum of GQD-30- C_{2v} (dibenzo[bc,ef]coronene, $C_{30}H_{14}$) computed using the PPP-CI method and the screened parameters (Fig. 4, main article). The rest of the information is same as in the caption of Table S1.

Peak	Symmetry	E (eV)	f	Wave function
I _x	1B_2	2.36	0.60	$ H \rightarrow L\rangle(0.8685)$ $ H - 2 \rightarrow L + 2\rangle(0.0634)$
II _y	1A_1	3.41	1.13	$ H - 1 \rightarrow L\rangle + c.c.(0.5907)$
III _y	1A_1	3.83	0.05	$ H \rightarrow L + 3\rangle + c.c.(0.5942)$
IV _x	1B_2	4.30	0.40	$ H - 1 \rightarrow L + 1\rangle(0.7471)$ $ H - 4 \rightarrow L\rangle + c.c.(0.1963)$
V _{xy}	1B_2	4.69	0.77	$ H - 2 \rightarrow L + 2\rangle(0.7999)$ $ H \rightarrow L; H \rightarrow L; H - 2 \rightarrow L + 2\rangle(0.1390)$
	1A_1	4.70	0.23	$ H - 6 \rightarrow L\rangle + c.c.(0.3107)$
VI _y	1A_1	4.93	0.32	$ H - 3 \rightarrow L + 2\rangle + c.c.(0.4402)$
VII _y	1A_1	5.23	0.22	$ H - 4 \rightarrow L + 1\rangle + c.c.(0.4897)$
VIII _y	1A_1	5.48	0.61	$ H - 1 \rightarrow L + 5\rangle + c.c.(0.4422)$
IX _x	1B_2	6.20	0.03	$ H \rightarrow L; H - 2 \rightarrow L + 1\rangle + c.c.(0.5387)$
X _x	1B_2	6.52	0.07	$ H - 4 \rightarrow L + 2\rangle + c.c.(0.3788)$

Table S6. Information regarding the excited states contributing to the peaks in the linear optical absorption spectrum of GQD-36- C_{2v} (dinaphtho[8,1,2abc;2',1',8'klm]coronene, $C_{36}H_{16}$) computed using the PPP-CI method and the standard parameters (Fig. 6, main article). The rest of the information is same as in the caption of Table S2.

Peak	Symmetry	E (eV)	f	Wave function
I _x	1B_2	3.22	0.08	$ H \rightarrow L\rangle(0.6964)$ $ H - 1 \rightarrow L + 1\rangle(0.4872)$
II _{xy}	1B_2	3.93	0.96	$ H - 1 \rightarrow L + 1\rangle(0.6650)$ $ H \rightarrow L\rangle(0.4766)$
	1A_1	3.99	0.59	$ H - 1 \rightarrow L\rangle + c.c.(0.4348)$
III _y	1A_1	4.31	0.35	$ H - 1 \rightarrow L\rangle + c.c.(0.3905)$
IV _x	1B_2	4.59	0.05	$ H - 5 \rightarrow L + 1\rangle + c.c.(0.4965)$
V _y	1A_1	4.95	0.46	$ H - 5 \rightarrow L\rangle + c.c.(0.3600)$
VI _x	1B_2	5.07	0.27	$ H - 1 \rightarrow L + 2\rangle + c.c.(0.4051)$
VII _y	1A_1	5.41	0.14	$ H - 4 \rightarrow L + 1\rangle + c.c.(0.5341)$
VIII _y	1A_1	5.77	0.21	$ H - 5 \rightarrow L\rangle + c.c.(0.4114)$
IX _x	1B_2	6.00	0.70	$ H - 4 \rightarrow L + 4\rangle(0.3526)$ $ H - 6 \rightarrow L + 1\rangle + c.c.(0.3099)$
X _{xy}	1B_2	6.32	0.48	$ H - 3 \rightarrow L + 3\rangle(0.4172)$ $ H - 4 \rightarrow L + 4\rangle(0.3191)$
	1B_2	6.41	0.47	$ H - 2 \rightarrow L + 5\rangle + c.c.(0.3571)$
	1A_1	6.49	0.90	$ H - 2 \rightarrow L + 3\rangle + c.c.(0.4692)$
XI _x	1B_2	6.74	0.26	$ H - 4 \rightarrow L + 4\rangle(0.3329)$ $ H \rightarrow L + 11\rangle + c.c.(0.2803)$

Table S7. Information regarding the excited states contributing to the peaks in the linear optical absorption spectrum of GQD-36- C_{2v} (dinaphtho[8,1,2abc;2',1',8'klm]coronene, $C_{36}H_{16}$) computed using the PPP-CI method and the screened parameters (Fig. 6, main article). The rest of the information is same as in the caption of Table S2.

Peak	Symmetry	E (eV)	f	Wave function
I _x	1B_2	2.91	0.86	$ H \rightarrow L\rangle(0.8599)$ $ H - 1 \rightarrow L + 1\rangle(0.0520)$
II _{xy}	1A_1	3.17	1.09	$ H \rightarrow L + 1\rangle + c.c.(0.6011)$
	1B_2	3.19	1.06	$ H - 1 \rightarrow L + 1\rangle(0.8517)$ $ H - 1 \rightarrow L + 2\rangle + c.c.(0.0659)$
III _{xy}	1A_1	3.92	0.04	$ H - 2 \rightarrow L\rangle + c.c.(0.5742)$
	1B_2	4.00	0.31	$ H - 2 \rightarrow L + 1\rangle + c.c.(0.5288)$
IV _y	1A_1	4.22	0.12	$ H - 1 \rightarrow L + 3\rangle + c.c.(0.5328)$
V _{xy}	1B_2	4.40	0.16	$ H \rightarrow L + 4\rangle + c.c.(0.5655)$
	1A_1	4.46	0.27	$ H - 4 \rightarrow L + 1\rangle + c.c.(0.4720)$
VI _y	1A_1	5.07	0.70	$ H - 3 \rightarrow L + 2\rangle + c.c.(0.5427)$
VII _x	1B_2	5.33	0.72	$ H - 4 \rightarrow L + 3\rangle + c.c.(0.4021)$
	1B_2	5.38	0.61	$ H - 1 \rightarrow L + 8\rangle + c.c.(0.3833)$
VIII _x	1B_2	5.66	0.08	$ H - 4 \rightarrow L + 4\rangle(0.7716)$ $ H - 4 \rightarrow L + 3\rangle + c.c.(0.2137)$
	1A_1	6.07	0.03	$ H \rightarrow L; H \rightarrow L + 3\rangle + c.c.(0.5153)$
IX _y	1A_1	6.35	0.04	$ H - 6 \rightarrow L\rangle + c.c.(0.4991)$

Table S8. Information regarding the excited states contributing to the peaks in the linear optical absorption spectrum of GQD-36- C_{2h} (dinaphtho[8,1,2abc;2',1',8'jkl]coronene, $C_{36}H_{16}$) computed using the PPP-CI method and the standard parameters (Fig. 8, main article). The rest of the information is same as in the caption of Table S3.

Peak	Symmetry	E (eV)	f	Wave function
I _{xy}	1B_u	2.97	0.41	$ H \rightarrow L\rangle(0.8163)$
				$ H - 1 \rightarrow L + 1\rangle(0.2750)$
II _{xy}	1B_u	4.05	1.97	$ H \rightarrow L + 1\rangle + c.c.(0.5634)$
III _{xy}	1B_u	4.37	0.47	$ H - 2 \rightarrow L + 2\rangle(0.4453)$
				$ H - 1 \rightarrow L + 1\rangle(0.4182)$
IV _{xy}	1B_u	4.66	0.62	$ H - 1 \rightarrow L + 1\rangle(0.5869)$
				$ H - 5 \rightarrow L\rangle + c.c.(0.3604)$
V _{xy}	1B_u	5.34	0.31	$ H \rightarrow L + 8\rangle + c.c.(0.3657)$
VI _{xy}	1B_u	5.48	0.64	$ H - 2 \rightarrow L + 2\rangle(0.5942)$
				$ H - 1 \rightarrow L + 1\rangle(0.3272)$
VII _{xy}	1B_u	5.82	0.28	$ H - 7 \rightarrow L + 2\rangle + c.c.(0.2774)$
VIII _{xy}	1B_u	6.10	0.65	$ H - 1 \rightarrow L + 5\rangle + c.c.(0.3209)$
IX _{xy}	1B_u	6.47	0.67	$ H - 4 \rightarrow L + 4\rangle(0.5862)$
				$ H - 8 \rightarrow L + 1\rangle + c.c.(0.2342)$
	1B_u	6.51	0.71	$ H - 1 \rightarrow L + 5\rangle + c.c.(0.3351)$

Table S9. Information regarding the excited states contributing to the peaks in the linear optical absorption spectrum of GQD-36- C_{2h} (dinaphtho[8,1,2abc;2',1',8'jk]coronene, $C_{36}H_{16}$) computed using the PPP-CI method and the screened parameters (Fig. 8, main article). The rest of the information is same as in the caption of Table S3.

Peak	Symmetry	E (eV)	f	Wave function
I _{xy}	1B_u	2.53	0.62	$ H \rightarrow L\rangle(0.8661)$ $ H - 1 \rightarrow L + 1\rangle(0.0735)$
II _{xy}	1B_u	3.22	1.98	$ H \rightarrow L + 1\rangle + c.c.(0.6136)$
III _{xy}	1B_u	3.93	0.41	$ H - 1 \rightarrow L + 1\rangle(0.8552)$ $ H - 2 \rightarrow L + 2\rangle(0.1195)$
IV _{xy}	1B_u	4.33	0.67	$ H - 2 \rightarrow L + 2\rangle(0.7508)$ $ H - 5 \rightarrow L\rangle + c.c.(0.2902)$
V _{xy}	1B_u	4.79	0.21	$ H - 4 \rightarrow L + 2\rangle + c.c.(0.3566)$
VI _{xy}	1B_u	5.03	0.69	$ H - 5 \rightarrow L + 1\rangle + c.c.(0.3672)$
VII _{xy}	1B_u	5.75	0.07	$ H - 7 \rightarrow L + 2\rangle + c.c.(0.5930)$